Effect of a quenched random field on a continuous symmetry breaking transition: Nematic to smectic-*A* transition in octyloxycyanobiphenyl-aerosil dispersions

P. S. Clegg, C. Stock, and R. J. Birgeneau
Department of Physics, University of Toronto, Toronto, Ontario, Canada M5S 1A7

C. W. Garland
Department of Chemistry, Massachusetts Institute of Technology, Cambridge, Massachusetts 02139

A. Roshi and G. S. Iannacchione
Department of Physics, Worcester Polytechnic Institute, Worcester, Massachusetts 01609

High-resolution x-ray diffraction and ac-calorimetric experiments have been carried out on the liquid-crystal octyloxycyanobiphenyl in which aerosil particles are dispersed. The measurements were made over a temperature range around the bulk nematic to smectic-*A* transition temperature. At this transition the liquid crystal breaks translational symmetry in a single direction. The silica particles, which hydrogen bond together to form a very low density gel, provide the quenched disorder. The random gel leads to observable broadening of the x-ray reflection from the smectic layers. The structure factor is well described by modeling the effect of the aerosils as a quenched random field. Dispersed aerosils are thought to pin both the direction of the translational ordering and the position of the layers. The latter appears to have the greatest effect on the x-ray line shape. We show that the aerosil surface area, as verified by small-angle scattering, equates to the variance of the random field. Calorimetric results reveal substantial change in the specific heat peak associated with the nematic to smectic-*A* transition. As the concentration of aerosil increases, the specific heat peak remains sharp yet decreases in magnitude and shifts in temperature in a nonmonotonic fashion. In this regime, the critical exponent α becomes progressively smaller. For the samples with the largest concentrations of aerosil particles the $C_p(N\text{-}A)$ peak becomes highly smeared and shifts smoothly to lower temperatures.

I. INTRODUCTION

Recent studies of the nematic (*N*) to smectic-*A* (Sm*A*) transition in octylcyanobiphenyl (8CB)-aerosil dispersions by Park and co-workers using x-ray scattering [1,2] and by Iannacchione and co-workers using calorimetry [3] have shown that this system has clear quenched random-field characteristics and that the finite ordered domain size creates finite-size scaling effects [4]. Here we present a complementary study of a different liquid crystal—octyloxycyanobiphenyl (8OCB). Measurements on 8OCB enable us to test further our understanding of liquid-crystal–aerosil dispersions. This material has a wider nematic range than 8CB; it has larger elastic constants in the nematic phase and, has a smectic phase that is more sensitive to changes in density. The final point is illustrated by the reentrant nematic phase that 8OCB exhibits at high pressures or when diluted with a shorter homolog [5].

The effect of quenched disorder on phase transition behavior can be profound. Of interest here is quenched random disorder that couples linearly to the order parameter. We have studied the effect of this apparent random field on the nematic to smectic-*A* (*N*-Sm*A*) phase transition in the liquid-crystal material 8OCB. The smectic order parameter involves the amplitude and the phase of a one-dimensional density wave [6]; this is a three-dimensional (3D) two-component order-parameter system.

The molecule 8OCB has a rigid biphenyl core, a polar cyano head, and an aliphatic tail. At ∼353 K there is a transition from the isotropic to the nematic phase. Below this

temperature the molecules become orientationally ordered. At $T_{N\text{-}A}^0 \simeq 340$ K a transition occurs from the nematic to a partial bilayer smectic-*A* phase. The 1-atm phase sequence for 8OCB is [7]

$$\text{Crystal} \xrightarrow{\sim 327.9 \text{ K}} \text{Sm}A_\text{d} \xrightarrow{340.27 \text{ K}} N \xrightarrow{353.39 \text{ K}} I,$$
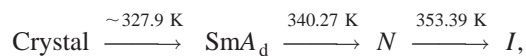
where the reproducible crystal-Sm*A* melting temperature is given. Due to coupling between the nematic order parameter and the smectic order parameter as well as couplings involving the fluctuations, the nematic to smectic-*A* transition is not a simple member of the 3D-*XY* universality class. Rather, it exhibits complex anisotropic critical behavior [8].

The effects of random fields on single component order-parameter magnetic transitions have been studied for many years [9]. This has been carried out using the Fishman-Aharony trick: a random-field Ising ferromagnet can be created by applying a magnetic field to a diluted Ising antiferromagnet [10]. However, it is not possible to use this technique for systems with more than a single order-parameter component. The applied field will always result in a uniaxial random field rather than matching the symmetry of the system. Common realizations of multicomponent order-parameter random-field systems are pinned vortices in type II superconductors [11] and pinned charge-density waves [12,13]. In both of these systems, the disorder strength is substantially more difficult to control than the applied magnetic field in the random-field Ising model (RFIM) systems.

The nematic to smectic-*A* transitional behavior in pure liquid crystals has been studied extensively using high-

resolution x-ray diffraction. An attractive feature of studying the effect of disorder on liquid-crystal behavior is the precision with which the pure system structure factor is known. High-resolution measurements have demonstrated that the smectic correlations in the nematic phase are described by an anisotropic Lorentzian structure factor [14]. The results clearly show that a fourth-order correction term is required, which diminishes as the transition is approached. Although this behavior is well characterized empirically, it is not yet fully understood.

The study of the nematic to smectic-*A* transition in a random field presented here is important because it is a multicomponent order-parameter system for which the disorder strength can be easily controlled. The quenched random field is created by a gel of aerosil particles. The strength and orientation of the *field* are random with a mean value of zero. The scale of the perturbation is parametrized in terms of its variance which can be varied by changing the density of aerosils in the dispersion. The aerosils are silica spheres of about 70-Å diameter; they hydrogen bond together to form a random gel. Studies have previously been carried out by various groups on liquid crystals in an aerogel medium [15–17]. Using aerosil as the disordering medium facilitates the creation of gels with a higher pore volume fraction and thus opens up a physically interesting regime. The aerosil or aerogel surface pins both the direction of the layer normal and the position of the layers. Small-angle x-ray studies have shown that the aerosil dispersion has a fractal structure and has no preferred orientation [3]. Since the fractal correlations are on much longer length scales than the smectic order, the gel surfaces are effectively uncorrelated. The random surfaces provide a random pinning field, overcoming the intrinsic problem with magnetic systems.

To understand the effect of the aerosil network on the *N*-Sm*A* transition, it is necessary to first consider how the disorder disrupts the orientationally ordered nematic phase. The aerosil network dilutes the nematogens and additionally creates a preferred orientation [18,19]. The latter effect is the most important and contributes to the total free energy as

$$F_r^N = \int d^3x [-g_2(\mathbf{h}\cdot\mathbf{n})^2], \qquad (1)$$

where $\mathbf{n}$ is the orientation of the molecules and $\mathbf{h}$ is the random influence of the sil surface. This term is squared due to the effective inversion symmetry of the molecules in the nematic phase. Since the nematic order parameter is quadratic in $\mathbf{n}$, this term is linear in the nematic order parameter and hence this constitutes a random field. In support of this conjecture, light scattering measurements show that the nematic phase in liquid-crystal aerosil dispersions breaks up into large but finite-sized domains [20–22]. As the sample is cooled further, smectic correlations develop within finite-sized nematic domains. The free energy of the liquid crystal close to the *N*-Sm*A* transition can be written as the sum of the de Gennes free energy, the Frank free energy for director fluctuations, and the contribution due to the influence of aerosil. The latter can be expressed as [18,23]

$$F_r^{SmA} = \int d^3x [-g_2(\mathbf{h}\cdot\mathbf{n})^2 - V\psi - V^*\psi^*]. \qquad (2)$$

Here $\mathbf{n}$ is again the director while ψ is the complex order parameter for the smectic-*A* phase. The first term is the continued influence of the aerosil surface on the molecular orientations. This interaction limits the ability of the smectic correlations to increase the nematic order. It also modifies the relationship between the nematic and smectic phases and as a result makes the system behave more like a standard 3D-*XY* system [3]. The second pair of terms represent the influence of the aerosil environment on the position of the smectic layers. This term is linear in the smectic order parameter ψ and is likely to create the observed random-field behavior. The pinning of the layer position at the *N*-Sm*A* transition is similar to the pinning of the phase of a charge-density wave by random impurities.

Previously, 8CB-aerosil dispersions have been studied using high-resolution x-ray diffraction [1,2]. The structure factor used to analyze the scattered intensity as a function of wave-vector transfer was motivated by analogy with the behavior of magnetic random-field systems. This appears to support the idea that the aerosil network creates a quenched random pinning field. The correlation length for smectic fluctuations was observed to saturate at a finite value that was density dependent. Thus no true Sm*A* phase exists in aerosil samples. However, there is an *effective N*-Sm*A* transition temperature T^*, below which static quenched-random effects dominate and above which they are close to negligible and thermal fluctuations dominate. The smectic domains that form are much smaller than the nematic domains that precede them [1,2] (the nematic correlation length $\xi_N \geq 5\bar{\xi}$, where $\bar{\xi}$ is the orientationally averaged smectic-*A* correlation length at low temperatures [22]). Here we build on the 8CB-aerosil work by showing that the dependence of the x-ray scattering for 8OCB on the aerosil concentration is also in agreement with theoretical expectations. We will discuss the similarities and differences between the responses of these two systems to the quenched disorder.

Other studies have been carried out on liquid crystals with an aerosil dispersion using a variety of techniques. Calorimetry measurements on 8CB with an aerosil dispersion have yielded detailed information on both the nematic to isotropic (*N*-*I*) transition and the *N*-Sm*A* transition [3]. Deuterium nuclear magnetic resonance (DNMR) measurements have also been made on 8CB with an aerosil dispersion [24]. Both calorimetry and DNMR results are consistent with a model in which the nematic susceptibility decreases with increasing aerosil density.

Promising results have been obtained concerning the dynamical behavior of 8CB-aerosil dispersions using x-ray intensity fluctuation spectroscopy [25]. Measurements of the aerosil dynamics were carried out with x-ray energies just below the Si absorption edge and in a wave-vector range sensitive to the large-scale silica gel structure. The results show that the silica gel motions are damped by the liquid-crystal elastic medium and that the relaxation time constant increases substantially at the *N*-Sm*A* transition.

TABLE I. Parameters for seven 8OCB-aerosil dispersions studied with x rays. Shown are densities ρ_S and ρ_P in g of SiO_2 per cm^3 of 8OCB; ratio of transmitted to incident beam intensity $I/I(0)$; thickness d in mm; ratio of random-field amplitude a_2 to thermal amplitude σ_1 at low temperature (LT) in units of 1×10^{-5} Å^{-1}; low-temperature parallel correlation length ($\xi_\parallel$) in Å and, pseudotransition temperature (T^*) in K.

ρ_S	ρ_P	$I/I(0)$	d	a_2/σ_1 (LT)	$\xi_\parallel$ (LT)	T^*
0.025	0.027 ± 0.001	0.46	1.46			340.02 ± 0.03
0.051	0.045 ± 0.002	0.65	0.70	0.042 ± 0.010	3670 ± 10	340.04 ± 0.07
0.078	0.076 ± 0.003	0.54	0.87	0.022 ± 0.010	3290 ± 10	339.81 ± 0.10
0.105	0.108 ± 0.004	0.37	1.28	0.026 ± 0.007	2995 ± 10	336.06 ± 0.10
0.220	0.238 ± 0.008	0.34	0.97	0.273 ± 0.056	965 ± 5	338.24 ± 0.06
0.347	0.341 ± 0.011	0.22	1.06	0.429 ± 0.131	820 ± 5	337.67 ± 0.47
0.489	0.343 ± 0.034	0.41	0.51	5.25 ± 1.82	410 ± 5	337.30 ± 1.61

This paper is organized as follows. Section II describes the preparation of the 8OCB-aerosil dispersions. In addition, the configurations for the high-resolution x-ray diffraction measurements and the ac calorimetry techniques will be described. Given in Sec. III is a presentation of the results and a description of the data analysis. The choice of x-ray line shape is motivated by results with 8CB and from magnetic RFIM systems. The correlation lengths and peak intensities derived as a result are shown as a function of the aerosil density, which is proportional to the silica aerosil surface area. The dependence on aerosil density of the N-SmA specific heat peak and enthalpy are also presented. All results are then discussed in Sec. IV and related to results from previous aerogel and aerosil studies and to theoretical predictions. The discussion section includes suggested directions for further study.

II. EXPERIMENTAL TECHNIQUES

The 8OCB liquid crystal was used as purchased from Aldrich. Type 300 aerosils, hydrophilic due to a surface coating of hydroxyl groups, were obtained from Degussa [26]. The specific surface area measured by the manufacturer via Brunauer-Emmett-Teller isotherms is 300 $m^2 g^{-1}$, each particle having a roughly 70-Å diameter. Prior to dispersal, the aerosils were dried by heating on a hot plate to ~ 570 K under vacuum. The appearance changes from being highly *fluffy* to being more powderlike when dry. The seven different density samples studied with x rays are listed in Table I. Each was created by mixing appropriate quantities of liquid crystal and aerosils. The density is quantified as ρ_S, the mass of aerosil divided by the volume of liquid crystal [3], which is related to the surface area of the random gel. The resulting mixture was dissolved in high-purity ethanol with very low water content, and the solution was then dispersed using an ultrasonic bath for about an hour. As the solvent slowly evaporates from the mixture, a fractal-like gel begins to form. The aerosil particles hydrogen bond together to give the structure that is disordered on the length scales of interest here. At room temperature 8OCB is a crystalline solid. It was imperative to avoid crystallization of the 8OCB once an aerosil dispersion is formed, since this was observed to give rise to phase separation in the sample. While the ethanol was

being evaporated, the samples were kept on a hot plate at ~ 338 K to insure that crystallization was avoided.

For the calorimetric study, rapid cooling of the sample and cell (in seconds) due to its small mass prevented the use of the approach detailed above. Instead, the sample was prepared in high-purity acetone and after the solvent evaporated was allowed to crystallize. The solid sample was transferred to the calorimetry cell, sealed, and the heater and the thermometer attached. Then the cell was heated above T_{N-I} by passing a constant calibrated current through the heater, and the cell was placed in an ultrasound bath for over an hour to remix the sample directly within the cell. By maintaining current through the heater, the cell and sample's temperature was kept elevated while mounting into the calorimeter. Thus, there is a small difference in sample preparation between the x-ray and ac-calorimetric studies.

A. X-ray details

The high-resolution x-ray diffraction measurements were carried out at the X20A beam line at the National Synchrotron Light Source. This is a bending magnet beam line and in this case the energy (wavelength) was chosen to be 8 keV (~ 1.54 Å). The monochromatic incident beam was collimated using slits while the diffracted beam was collimated using slits and the (111) reflection of a Ge single crystal. The liquid-crystal–aerosil dispersion has a random isotropic distribution of domains. Smectic fluctuations give rise to a ring of scattering. The resolution along the radius of the ring was $\Delta 2\theta \sim 0.02°$.

The sample environment for the x-ray measurements comprised a single stage oven within a dry nitrogen environment. The sample temperature was controlled via a resistive heater stabilized by a proportional and integral controller to better than ± 0.05 K. The diffraction measurements were necessarily carried out in transmission geometry. The sample was sandwiched between two Kapton windows and had a diameter of ~ 5 mm and a thickness of ~ 1 mm. Care was taken that the sample remained well above the freezing temperature as it was transferred to the diffractometer.

Prior to taking data, each sample was held in the I phase at ~ 353 K for 6 h to allow the gel to equilibrate in the holder. Measurements of the line shape corresponding to smectic correlations were made over a range of temperatures down to 315 K. Cooling was carried out at a rate $\leqslant 1$ K h^{-1}.
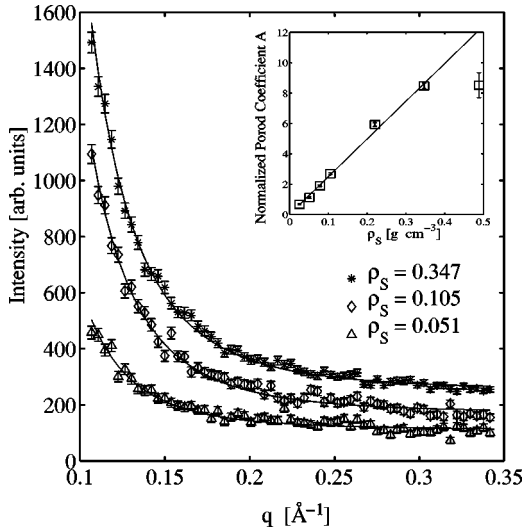
FIG. 1. X-ray scattering intensity as a function of wave-vector transfer for three 8OCB-aerosil dispersions at 353 K, which is ~ 13 K above the N-SmA transition temperature $T_{N\text{-}A}^0$ in pure 8OCB. The scattering is predominantly due to the aerosil particles and corresponds well to Porod's law: $I(q) = A/q^4 + B$. Inset: a plot of the q^{-4} coefficient A, corrected for absorption and normalized to the volume of liquid crystal, against ρ_S, the mass of aerosil per volume of liquid crystal.

The number of scans of intensity as a function of 2θ was kept limited and the counting time low in order to minimize the amount of x-ray damage. The sample thickness was varied with density in an effort to ensure that approximately one absorption length of material was in the beam. This was carried out so as to improve measurement statistics and to decrease the effects of beam damage.

Key parameters that characterize the composition and size of each sample are listed in Table I. The first column is the density ρ_S in g of SiO$_2$ per cm^3 of 8OCB. The second column is an empirical determination of ρ_S from the background scattering and is designated ρ_P. In addition to studying the smectic correlations as a function of temperature, measurements were made of the small-angle background scattering and of the absorption in the sample. The small-angle background scattering primarily results from the aerosil network. The intensity as a function of wave-vector transfer is plotted in Fig. 1 for a range of aerosil densities. These measurements were made at 353 K to minimize the contribution of smectic correlations to the scattered intensity. The wave-vector dependence of the intensity is well modeled by the Porod law [27]:

$$I(q) = \frac{A}{q^4} + B. \tag{3}$$

The parameter A is proportional to the total surface area of the scattering objects while parameter B is the wave vector independent background, which is likely to be due to both disordered liquid crystal and air scattering. The density ρ_S is the mass of aerosil per volume of liquid crystal and is proportional to the surface area of the aerosil particles. The values of the parameter A can be related to ρ_S values by correcting for absorption, dividing by the volume of liquid crystal and then finding the optimum proportionality constant using a least-squares fit; in this form they are listed in Table I. The fit results are shown in the inset to Fig. 1 and indicate good agreement between the experimental ρ_S values and the ρ_P values derived from Eq. (3). The relationship breaks down for the highest density. In this case the very small volume of liquid crystal in the beam results in substantial errors in the value of ρ_P.

Also listed in Table I are the ratios of the transmitted to the incident intensity and the thickness of the sample derived from this ratio. The ratio was determined by measuring the straight-through beam intensity in the absence of the sample, $I(0)$, and the straight-through beam intensity with the sample in place, I. For accurate measurements and minimal x-ray damage, the optimal sample thickness is such that on average each photon scatters once giving $I/I(0) \sim e^{-1}$. Our measured $I/I(0)$ values are scattered around 0.4, indicating close to optimal thickness.

B. Calorimetry details

High-resolution ac calorimetry was performed on two home-built calorimeters at WPI. The sample cell consisted of a silver crimped-sealed envelope ~ 10-mm long, ~ 5-mm wide, and ~ 0.5-mm thick (closely matching the dimensions of the heater). After the sample was introduced into a cell having an attached 120-Ω strain-gauge heater and 1-MΩ carbon-flake thermistor, a constant current was placed across the heater to maintain the cell temperature well above $T_{N\text{-}I}$. The filled cell was then placed in an ultrasonic bath to remix the sample. After remixing, the cell was mounted in the calorimeter, the details of which have been described elsewhere [28]. In the ac-mode, power is input to the cell as $P_{ac} e^{i\omega t}$ resulting in temperature oscillations with amplitude T_{ac} and a relative phase shift of $\varphi \equiv \Phi + \pi/2$, where Φ is the absolute phase shift between $T_{ac}(\omega)$ and the input power. The specific heat at a heating frequency ω is given by

$$C_p = \frac{[C'_{filled} - C_{empty}]}{m_{sample}} = \frac{P_{ac}\cos\varphi/\omega|T_{ac}| - C_{empty}}{m_{sample}}, \tag{4}$$

$$C''_{filled} = \frac{P_{ac}}{\omega|T_{ac}|}\sin\varphi - \frac{1}{\omega R}, \tag{5}$$

where C'_{filled} and C''_{filled} are the real and imaginary components of the heat capacity, C_{empty} is the heat capacity of the cell and silica, m_{sample} is the mass in grams of the liquid crystal (in this work, ~ 20 mg of 8OCB-aerosil sample, which corresponds to 13-20 mg of 8OCB), and R is the thermal resistance between the cell and the bath (here, ~ 200 K W^{-1}). Equations (4) and (5) require a small correction [28] in order to account for the finite internal thermal resistance compared to R, and this correction was made for all samples studied here [29]. Measurements were conducted at various frequencies in order to ensure the applicability of Eqs. (4) and (5) by checking that $C''_{filled} \approx 0$ through the effective N-SmA transition at T^* and that C_p was independent
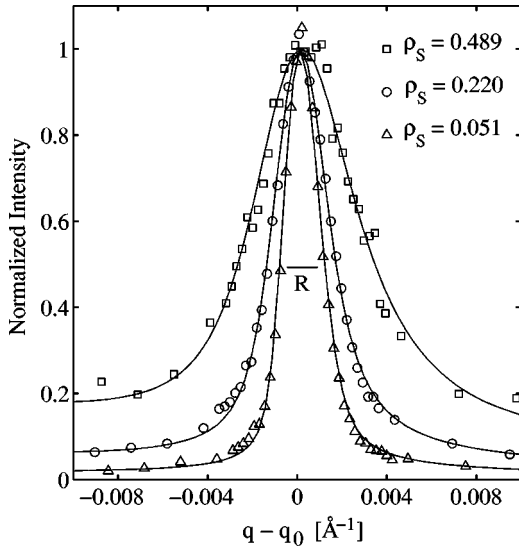
FIG. 2. Normalized x-ray scattering intensity of 8OCB-aerosil dispersions due to smectic-*A* order at low temperatures (approximately $T^0_{N\text{-}A} - 25$ K) versus wave-vector transfer. The broadening due to increasing disorder is evident. The lines are the results of fits to a model described in the text. The width of the resolution function is indicated by the horizontal line labeled *R*.

FIG. 3. Normalized x-ray scattering intensity due to short-ranged smectic-*A* order for an 8OCB-aerosil dispersion with $\rho_S = 0.105$ g cm^{-3} versus wave-vector transfer. The profile changes between $T = 338$ K $= T^* + 1.94$ K and $T = 315$ K $= T^* - 21.1$ K. The lines are the results of fits to a model described in the text.

of ω. All data presented here were taken at $\omega = 0.1473$ s^{-1} at a scanning rate of less than ± 100 mK h^{-1}, which yield essentially static C_p results. All 8OCB-aerosil samples experienced the same thermal history after mounting; 6 h in the isotropic phase to ensure homogeneous gelation, then a slow cooling deep into the smectic phase before beginning the first detailed scan upon heating.

III. RESULTS

A. X-ray results

High-resolution x-ray diffraction measurements were carried out for 8OCB with the aerosil densities listed in Table I over the temperature range 353 to 315 K. Figure 2 shows the scattering intensity as a function of wave-vector transfer for three different aerosil densities. The displayed results are for the lowest temperature studied ($\sim T^0_{N\text{-}A} - 25$ K). The resolution width, determined from the profile of the straight-through beam, is indicated by a horizontal line. The addition of aerosil particles leads to peak broadening beyond the resolution limit even at the lowest temperature studied. Unfortunately, at the lowest density studied ($\rho_S = 0.025$ g cm^{-3}), any peak broadening is unresolvable for the beam profile available in this work. At higher densities of the aerosils, the peaks are broader than the resolution and thus the smectic correlation lengths are finite even at the lowest temperatures. There is a clear qualitative change in the reflection profile with increasing density; and the solid lines are the results of fits to a model of the x-ray scattering structure factor, which will be described below.

For each aerosil density the reflection line shape evolves as the temperature is reduced. Figure 3 shows the x-ray scattered intensity as a function of wave-vector transfer for two
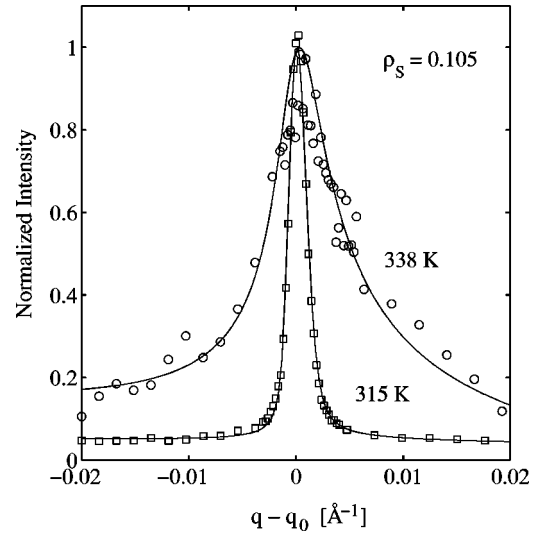
temperatures at the same aerosil density. At high temperatures (e.g., 338 K) short-range smectic fluctuations are evidenced by a broad peak in the scattered intensity. The reflection becomes narrower and sharper at lower temperatures. Again the solid lines are the results of fits with the model of the structure factor given below.

The x-ray structure factor for smectic thermal fluctuations has been studied intensively. The most commonly used expression is [14]

$$S^T(\mathbf{q}) = \frac{\sigma_1}{1 + \xi_\parallel^2 (q_\parallel - q_0)^2 + \xi_\perp^2 q_\perp^2 + c\xi_\perp^4 q_\perp^4}. \qquad (6)$$

This is an anisotropic Lorentzian with a fourth-order correction. $\xi_\parallel$ ($\xi_\perp$) is the correlation length parallel (perpendicular) to the smectic layers; q_0 ($2\pi/d$, where d is the smectic layer thickness) is the wave vector corresponding to the peak in the reflected intensity; σ_1 is related to the thermal fluctuation susceptibility; c gives the scale of the fourth-order correction. The coefficient c has the value ~ 0.25 at high temperatures, hence the perpendicular profile is a Lorentzian squared intensity distribution. c tends to 0 as the transition is approached. This line shape has been used to analyze x-ray scattering from pure 8OCB and many other smectic liquid crystals. The reduced temperature dependence of the fourth-order correction and the ratio $\xi_\perp / \xi_\parallel$ are consequently well known for 8OCB [30].

The x-ray structure factor used to analyze the scattering from the 8OCB-aerosil dispersions is motivated by studies of random-field magnets. A random field gives rise to fluctuations of the ordered state with a different wave-vector dependence than that for thermal fluctuations. Experimental studies [9] support the idea that random-field fluctuations behave like thermal fluctuations with the lower marginal dimensionality shifted up by two. This leads to the structure factor

$$S^{RF}(\mathbf{q}) = \frac{\sigma_2}{[1 + \xi_\parallel^2(q_\parallel - q_0)^2 + \xi_\perp^2 q_\perp^2 + c\xi_\perp^4 q_\perp^4]^2}. \quad (7)$$

The denominator is the square of the thermal fluctuation denominator. For $d \geq 4$ the dimensional change argument can be justified theoretically [31]. The numerator σ_2 is related to the disconnected susceptibility. Smectic correlations in the 8OCB-aerosil dispersions are influenced by both thermal fluctuations and the random-field fluctuations. Aharony and Pytte [32] have shown that for a random-field system the structure factor should have the low-temperature scaling form

$$S(q, \xi) = \xi^d \bar{S}(q\xi). \quad (8)$$

For smectic liquid-crystal fluctuations there are different correlation lengths in the directions parallel and perpendicular to the smectic layer normal. We assume by analogy with the isotropic result that the structure factor should have the scaling form

$$S(q_\parallel, \xi_\parallel, q_\perp, \xi_\perp) = \xi_\parallel \xi_\perp^2 \bar{S}(q_\parallel \xi_\parallel, q_\perp \xi_\perp). \quad (9)$$

Comparison of this form with Eq. (7) leads to the conclusion that, for a random-field system, the amplitude can be written as

$$\sigma_2 = a_2(\xi_\parallel \xi_\perp^2), \quad (10)$$

which defines the parameter a_2.

The total structure factor thus consists of two terms:

$$S(\mathbf{q}) = S^T(\mathbf{q}) + S^{RF}(\mathbf{q}). \quad (11)$$

The thermal structure factor dominates at high temperatures, while the random-field structure factor given by Eq. (7) dominates at low temperatures. There is a concurrent change in the reflection line shape as the balance between these two structure factors changes. It should be noted that Eq. (11) provides an excellent description of the x-ray line shape of 8CB-aerosil dispersions [1,2]. In order to compare this model with the data, it is necessary to perform a powder average and then to convolve the resulting line shape with the resolution function. The powder average involves integrating over the random orientations of the smectic domains, and the resolution function is measured as the profile of the straight-through beam. The handling of the resolution function follows that discussed in detail in Ref. [2]. In the present work, we implemented the powder average by recasting the integral as an ordinary differential equation and solving this using a commercial implementation of the Runge-Kutta method. In Refs. [1] and [2] the powder average was carried out by expanding the line shape as a series and then evaluating the integral analytically. The performance of these two approaches has been compared for 8CB-aerosil data and has been found to be fully consistent.

The powder average of the structure factor given by Eq. (11) has been fitted to the measured wave-vector transfer dependence of the scattered intensity. The background intensity was taken to be a straight line

$$I^{Bk}(q) = Mq + C \quad (12)$$

over the limited $q - q_0$ range of the smectic scattering. Note that M is negative. The free parameters over which the fit is optimized are $M, C, q_0, a_1(= \sigma_1/\xi_\parallel \xi_\perp^2), a_2, \xi_\parallel$. The values of $\xi_\perp(\xi_\parallel)$ and $c(\xi_\parallel)$ are assumed to retain the same behavior as they exhibit in pure 8OCB. This assumption is physically reasonable for the weak disorder imposed by the aerosil gel and was also used for the 8CB-aerosil study [2]. An initial fitting of the data was made with all six parameters free. Subsequently, M and C were held fixed at their low-temperature average values for each sample to remove any unphysical fit noise. The remaining four parameters $q_0, a_1, a_2, \xi_\parallel$ were then redetermined. A background fixed at its low-temperature best fit parameters is chosen in preference to a high-temperature background in order to reduce the influence of scattering from the disordered liquid crystal. This approach yielded low χ^2 values [33]. The temperature and density dependence of $q_0, \sigma_1, a_2, \xi_\parallel$ are discussed below. The low-temperature limiting values of various parameters are shown in Table I. Examples of the correspondence between this structure factor and the measurements are given in Fig. 2 for different densities and in Fig. 3 for different temperatures. The agreement between the data and the model is observed to be good.

The peak position q_0, and its temperature dependence display little variation between samples for all densities except the highest value studied. For $\rho_S = 0.489$ g cm^{-3}, q_0 is slightly but noticeably lower (by ~ 0.0007 Å^{-1}) at all temperatures. For all other 8OCB-aerosil samples, the q_0 value varied from 0.1981 ± 0.0002 Å^{-1} at T_{N-A}^0 to 0.1998 ± 0.0002 Å^{-1} at $T_{N-A}^0 - 25$ K, and this weak common trend with temperature is completely analogous to that shown for 8CB-aerosil dispersions in Fig. 6 of Ref. [2]. The robust value of the peak position for low disorder is surprising. Pure 8OCB exhibits a partial bilayer smectic-*A* phase, hence the ordering wave vector is incommensurate with the molecular length. Since the balance of interactions in the liquid-crystal system is likely to be altered by the silica it might have been anticipated that the peak position would change for even the lowest ρ_S samples. The independence of $q_0(T)$ on ρ_S up to 0.347 g cm^{-3} demonstrates that the partial bilayer smectic in 8OCB-aerosil dispersions, although not long range, has the same local packing as in pure bulk 8OCB.

Figure 4 presents the results for the peak amplitudes. The parameter a_2 is close to the integrated intensity for the random-field contribution, Eq. (7); the temperature dependence of a_2 multiplied by a c-dependent correction is shown in Fig. 4(a) for three of the aerosil densities studied. Note that, as with 8CB-aerosil dispersions, there is an effective transition temperature T^*, below which static quenched-random effects dominate and above which they are negligible.

The thermal fluctuation term given in Eq. (6) would also describe the pretransitional behavior of a pure liquid crystal. The observed behavior of σ_1 is shown in Fig. 4(b). It was not possible to make sufficient measurements to explore fully the high-temperature behavior without subjecting the sample to
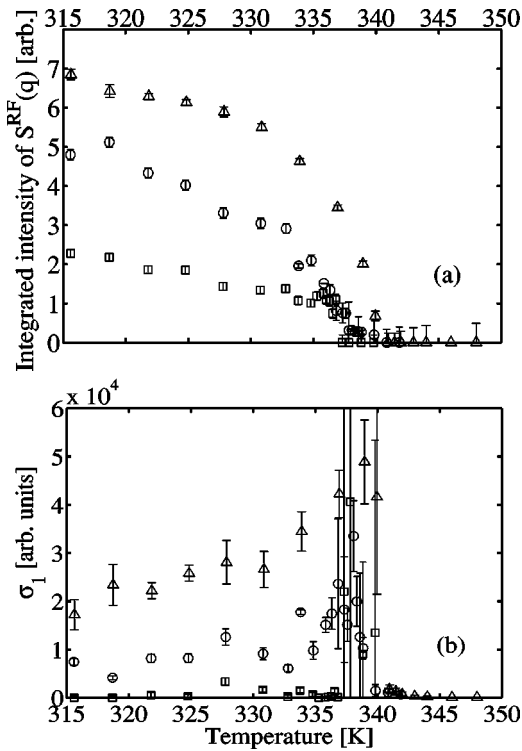
FIG. 4. (a) Integrated intensity of the random-field term $S^{RF}(\mathbf{q})$ versus temperature. (b) The amplitude of the thermal contribution to the scattering versus temperature. The $\rho_S = 0.220$ g cm^{-3} values have been multiplied by 2 and the $\rho_S = 0.489$ g cm^{-3} by 20.

FIG. 5. Variation of a_2/σ_1(LT) versus ρ_S. The full circles are for 8OCB-aerosil while the open circles are for 8CB-aerosil [4]. For 8OCB a_2 and σ_1 are the average values for $T < 320$ K, i.e., $\Delta T = T - T^* \sim -21$ K. The data points show large scatter but are roughly consistent with a_2/σ_1(LT) $\sim \rho_S^3$ (solid line).

excessive x-ray damage. Three densities are shown in Fig. 4(b), and in general the amplitude rises to a maximum around the pseudotransition temperature before settling toward a constant low-temperature plateau value. The maxima near T^* could be the remnants of the divergent susceptibility at the pure nematic to smectic-A transition.

At high temperatures the scattering is dominated by the thermal fluctuations while the random-field fluctuations dominate as T falls below an effective transition temperature T^*. It has been shown in Ref. [2] that the temperature dependence of a_2 can be represented by an effective power law $(T^* - T)^x$, where T^* marks the temperature above which the integrated intensity of the random-field component S^{RF} is essentially zero, as shown for 8OCB in Fig. 4(a). With both 8OCB-aerosil and 8CB-aerosil [1,2] studies the number of scans of scattered x-ray intensity was kept limited in order to minimize damage to the sample. For the 8CB-aerosil samples it was possible to make measurements down to ~ 15 K below T^* and hence the data are somewhat focused around the pseudotransition. With the 8OCB-aerosil samples measurements were made down to ~ 23 K below T^*. This has the advantage that the line shape can be characterized well below the pseudotransition and the disadvantage that there are fewer scans around the pseudotransition region itself. As a result, the present 8OCB-aerosil data are too sparse to yield a good set of values for the exponent x as a function of ρ_S; they can, however, be used to determine T^* values and these are given in Table I.
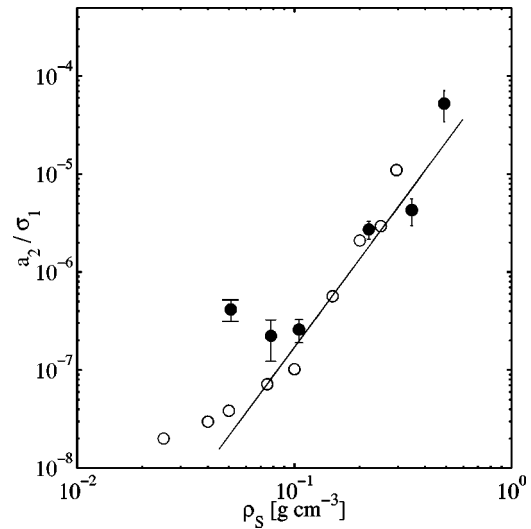
The amplitude ratio of the random-field term to the ther-

mal term far below the pseudotransition is predicted to be related to the variance Δ of the random field [32]. It has been shown [4] that the relationship can be written as $a_2/\sigma_1 \sim \Delta^3$. Note that the quantity a_2/σ_1 is independent of the normalization of the intensities. The low-temperature ratios are taken to be a_2/σ_1(LT), where both parameters are the average values for $T < 320$ K, i.e., $\Delta T = T - T^* \sim -21$ K. While neither a_2 nor σ_1 are quite saturated at these temperatures, this is the best available comparison with the theory. The ratio values, given in Table I and displayed in Fig. 5, show qualitative agreement with the relation $a_2/\sigma_1 \sim \rho_S^3$. This relationship will be discussed in Sec. IV. Also shown in Fig. 5 are the a_2/σ_1(LT) values for 8CB-aerosil [4]. The two systems can be seen to show good agreement over most of the ρ_S range.

In our analysis, only the parallel correlation length $\xi_\parallel$ was taken as a free parameter; the relationship between $\xi_\parallel$ and $\xi_\perp$ was assumed to be the same as that for the pure 8OCB liquid crystal. The fit $\xi_\parallel$ values for three densities are shown in Fig. 6. The correlation length is observed to grow sharply on cooling towards the pseudotransition, but rather than diverging as in a pure material the value saturates and remains roughly constant at low temperatures. The saturation value decreases monotonically with increasing density. For high densities, where the scattering intensity was smallest, there was an occasional difficulty extracting an unambiguous correlation length in the transition region. This can be observed in Fig. 6 as the slight peak for $\xi_\parallel$ close to T^* for $\rho_S = 0.220$ g cm^{-3}; the associated error bars (not shown) for correlation lengths are large. The equivalent feature for the $\rho_S = 0.489$ g cm^{-3} sample has been removed from Fig. 6 for clarity. The average low-temperature (below 323 K) $\xi_\parallel$ values are listed for each density in Table I; they are shown as dashed lines in Fig. 6. Many models of the effects of disorder on phase transition behavior apply to systems where the cor-
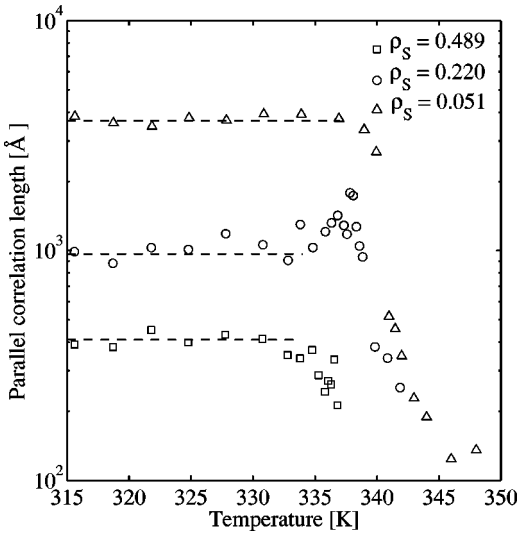
FIG. 6. Parallel correlation lengths for smectic order as a function of the temperature for three 8OCB-aerosil samples. The values saturate rather than diverge. The dashed lines show the low-temperature average values, $\xi_\parallel(LT)$, which are listed in Table I and described in the text.

FIG. 8. Specific heat due to the N-SmA phase transition, $\Delta C_p(N\text{-}A)$, as a function of temperature about T^* for bulk 8OCB and 8OCB-aerosil samples with densities from $\rho_S = 0.036$ to 0.647 g of silica per cm³ of liquid crystal. See figure inset for a definition of the symbols.

relation volume is isotropic. In order to make quantitative comparisons we assume that the cube root of the correlation volume gives the extent of SmA order. The values $\bar{\xi}^{LT} = (\xi_\parallel \xi_\perp^2)^{1/3}$ have been plotted in Fig. 7. The dependence of $\bar{\xi}^{LT}$ on ρ_S can be well described by the power law $\bar{\xi}^{LT} \sim \rho_S^\zeta$ with the exponent $\zeta \sim -1$. This relationship will be discussed in Sec. IV. Also shown in Fig. 7 are the $\bar{\xi}^{LT}$ values for 8CB-aerosil [4], which are in good agreement with the results presented here.
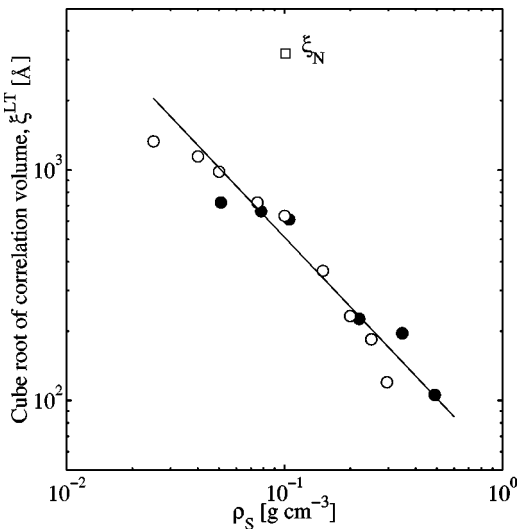
B. Calorimetric results

The heat capacity of the pure 8OCB liquid crystal used in making the 8OCB-aerosil samples was determined in order to make quantitative comparisons with aerosil data. The excess heat capacity associated with the N-SmA transition, shown in Fig. 8, is in good agreement with previously published results [7,34]. We find for our pure 8OCB material the transition temperatures $T_{N\text{-}I}^0 = 352.53$ K and $T_{NA}^0 = 339.52$ K. The N-I two-phase coexistence width was ≈ 95 mK, and the N-SmA transition enthalpy was $\delta H_{N\text{-}A}^0 = 0.42$ J g⁻¹. These thermal features indicate that the 8OCB material used for both x-ray and calorimetric studies was of reasonably good quality. A summary of the calorimetric results for our pure 8OCB and 8OCB-aerosil samples is given in Table II. Except for the additional $\rho_S = 0.036$ g cm⁻³ and

FIG. 7. Low-temperature correlation length for smectic order $\bar{\xi}^{LT} = (\xi_\parallel \xi_\perp^2)^{1/3}$ versus ρ_S. The full circles are for 8OCB-aerosil while the open circles are for 8CB-aerosil [4]. The power law shown by the line, which is $\bar{\xi}^{LT} \sim \rho_S^{-1}$, is expected for a random-field system if $\Delta \sim \rho_S$. The open square is the nematic correlation length ξ_N for 8CB-aerosil [22].
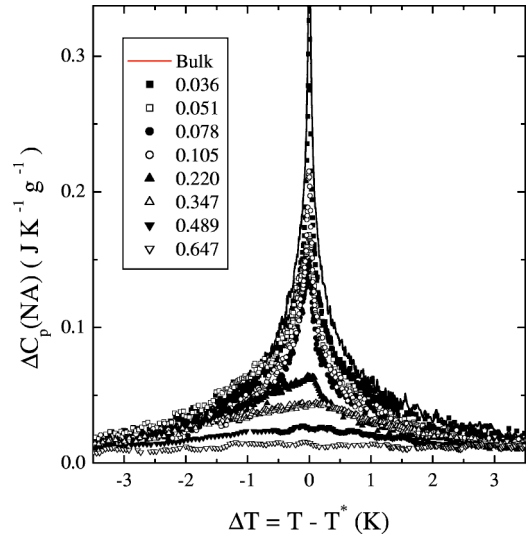
TABLE II. Summary of the heat capacity results for the 8OCB-aerosil samples. Shown are transition temperatures for the N-I ($T_{N\text{-}I}$) and the N-SmA (T^*) phase transitions in K, the nematic temperature range $\Delta T_{nem} = T_{N\text{-}I} - T^*$, the N-SmA transition enthalpy $\delta H_{N\text{-}A}$ in J g⁻¹, and heat capacity maximum (value at T^*) $h_M \equiv \delta C_p^{max}(N\text{-}A)$ in J K⁻¹ g⁻¹.

ρ_S	$T_{N\text{-}I}$	T^*	ΔT_{nem}	$\delta H_{N\text{-}A}$	$h_M \equiv \delta C_p^{max}(N\text{-}A)$
0	352.53	339.52	13.01	0.420	
0.036	352.53	339.64	12.89	0.385	0.326
0.051	352.79	340.22	12.57	0.334	0.167
0.078	351.08	338.61	12.47	0.268	0.146
0.105	351.02	338.51	12.51	0.284	0.213
0.220	351.20	338.61	12.59	0.230	0.100
0.347	352.31	338.85	13.46	0.202	0.044
0.489	352.05	338.05	14.00	0.149	0.027
0.647	351.41	337.30	14.11	0.050	0.014

TABLE III. Results from fitting Eq. (16) to the N-SmA excess heat capacity $\delta C_p(N$-$A)$ of the 8OCB-aerosil samples. Units for T_c are in K, $A^\pm$ and B_c are in J K^{-1} g^{-1}, while $D^\pm$ are dimensionless.

ρ_S	T_c	α	A^+	A^-	D^+	D^-	B_c	χ_ν^2
0	339.519	0.18	0.103	0.101	1.871	2.253	-0.264	1.017
0.036	339.639	0.17	0.087	0.082	0.874	1.643	-0.189	1.147
0.051	340.215	-0.04	-1.321	-1.367	-0.179	-0.470	1.098	1.098
0.078	338.612	0.14	0.081	0.089	-0.159	1.371	0.160	1.157
0.105	338.508	-0.01	-4.979	-4.999	-0.121	-0.161	4.712	1.854

0.647 g cm^{-3} samples, the samples studied with calorimetry were from the same batches as those studied by x rays. However, as explained in Sec. II, the sample handling differed slightly.

In order to determine the excess heat capacity associated with the N-SmA transformation shown in Fig. 8, two backgrounds were subtracted. The total sample heat capacity over a wide temperature range had a linear background, C_p (background), subtracted to yield

$$\Delta C_p = C_p - C_p(\text{background}) \qquad (13)$$

as the excess C_p due to the N-I and N-SmA phase transitions. The excess C_p due to the N-SmA transition, $\Delta C_p(N$-$A)$, was found by subtracting a mimic function (a simple power law $C_{power}^{N\text{-}I}$) depicting the low-temperature $\Delta C_p(N$-$I)$ wing variation:

$$\Delta C_p(N\text{-}A) = \Delta C_p - C_{power}^{N\text{-}I}. \qquad (14)$$

The parameters for each 8OCB-aerosil sample of the empirical low-temperature $C_{power}^{N\text{-}I}$ wing were determined by fitting ΔC_p after removing a $T^* \pm 5$ K window of data related to the N-SmA contribution. See Fig. 1 given in Ref. [3] and accompanying text there for details about obtaining $\Delta C_p(N$-$A)$. The resulting $\Delta C_p(N$-$A)$ data are shown for pure 8OCB and all 8OCB-aerosil samples in Fig. 8, where the units are J K^{-1} per gram of liquid crystal. The N-SmA transition enthalpy is then given by

$$\delta H_{N\text{-}A} = \int \Delta C_p(N\text{-}A) dT, \qquad (15)$$

where consistent limits of the integration, ± 5 K about T^*, were used for all samples.

The behavior of $\Delta C_p(N$-$A)$ as a function of temperature for various aerosil densities is shown in Fig. 8. The N-SmA C_p peak remains sharp for aerosil densities up to $\rho_S = 0.105$ g cm^{-3}. Above this aerosil density, $\Delta C_p(N$-$A)$ becomes significantly rounded. The increasingly asymmetric shape of $\Delta C_p(N$-$A)$ with increasing ρ_S, observed for 8CB-aerosils [3], is also observed for 8OCB-aerosil samples, though to a weaker extent. Since the change in shape for $\Delta C_p(N$-$A)$ has been interpreted as a disorder driven crossover toward the underlying 3D-XY critical behavior, the more subtle change for 8OCB-aerosil is not surprising as the bulk critical exponent for 8CB ($\alpha_{8CB} = 0.30$) is higher compared to that of 8OCB ($\alpha_{8OCB} = 0.20$ [8]). In this light, the

8OCB-aerosil system has to vary less in order to reach the 3D-XY fixed point ($\alpha_{3D\text{-}XY} = -0.013$).

To characterize the change in shape of these $\Delta C_p(N$-$A)$ data, a transitional power-law form [8] in terms of the reduced temperature $t = |T - T^*|/T^*$ is used to analyze the experimental specific heat data associated with the N-SmA phase transition:

$$\Delta C_p(N\text{-}A) = A^\pm t^{-\alpha}(1 + D^\pm t^{\Delta_1}) + B_c, \qquad (16)$$

where the critical behavior as a function of reduced temperature t is characterized by an exponent α, amplitudes $A^\pm$ above and below the transition, a critical background term B_c, and corrections-to-scaling terms characterized by the coefficients $D^\pm$ and exponent $\Delta_1 \simeq 0.5$. An increasing temperature gap of excluded data about the $\Delta C_p(N$-$A)$ peak with increasing ρ_S was required to perform the fitting. These fit results are presented in Table III and show a systematic evolution of the effective critical exponent α toward the 3D-XY value consistent with previous studies on 8CB-aerosil samples [3]. The exception is the $\rho_S = 0.051$ g cm^{-3} 8OCB-aerosil sample, which exhibits an exponent that does not fit well with the trend in the other α values, and this is possibly an indication that the sample in our cell had an inhomogeneous dispersion. This sample also strongly deviated from the general trend at the N-I transition.

The N-I and N-SmA transition temperatures, the nematic temperature range ΔT_{nem}, the N-SmA transition enthalpy $\delta H_{N\text{-}A}$, and the heat capacity maximum $h_M \equiv \delta C_p^{max}(N$-$A)$ are tabulated along with ρ_S in Table II for the 8OCB-aerosil dispersions studied by calorimetry. The N-SmA pseudotransition temperature T^*, and the transition enthalpy $\delta H_{N\text{-}A}$ can be normalized by the corresponding bulk values, $T_{N\text{-}A}^0$ and $\delta H_{N\text{-}A}^0$, respectively, in order to make quantitative comparison with the results for the previously studied 8CB-aerosil system [3].

The N-SmA transition enthalpy, as determined from Eq. (15), for the 8OCB-aerosil samples is sensitive to the changes in shape of the $\Delta C_p(N$-$A)$ peak and complements the power-law analysis of the evolving critical behavior. Here we take $\delta H_{N\text{-}A}^0 = 0.42$ J g^{-1} for our bulk 8OCB N-SmA transition enthalpy. These enthalpy results, scaled by the pure LC value, are shown versus ρ_S in Fig. 9 for 8OCB-aerosil and 8CB-aerosil samples. Note that the same fractional change in N-SmA enthalpy occurs for 8OCB-aerosil and 8CB-aerosil samples as a function of ρ_S. Two ρ_S regimes are evident. For $0 < \rho_S \lesssim 0.1$, there is a rapid drop in $\delta H_{N\text{-}A}$,
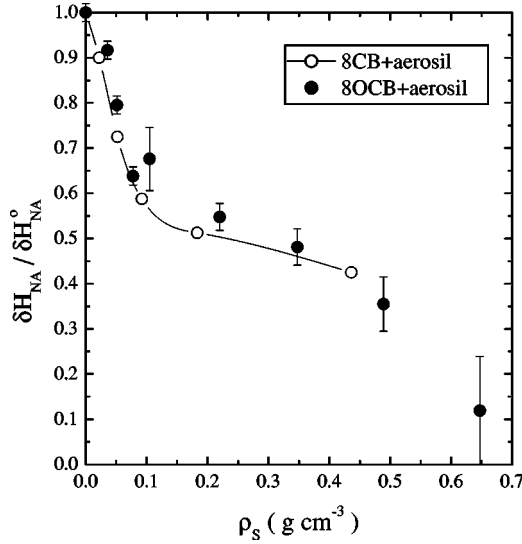
FIG. 9. The ρ_S dependence of the N-SmA pseudotransition enthalpy $\delta H_{N\text{-}A} = \int \Delta C_p(N\text{-}A) dT$ scaled by the transition enthalpy of pure 8OCB, $\delta H_{N\text{-}A}/\delta H_{N\text{-}A}^0$, for the 8OCB-aerosil samples. Also shown are $\delta H_{N\text{-}A}/\delta H_{N\text{-}A}^0$ for 8CB-aerosil samples taken from Ref. [3].

FIG. 10. Behavior of the N-SmA heat capacity maximum h_M $\equiv \Delta C_p^{max}(N\text{-}A)$ at T^* as a function of ρ_S for the 8OCB-aerosil samples and the 8CB-aerosil samples taken from Ref. [3]. The solid (dashed) line shows the finite-size scaling prediction for 8OCB (8CB) -aerosil samples.

while for ρ_S values greater than ~ 0.1 the decrease is more gradual. For the $\rho_S = 0.647$ g cm^{-3} sample, $\delta H_{N\text{-}A}$ has nearly disappeared indicating that the SmA absolute stability limit must be near this aerosil density for 8OCB-aerosil samples.

Values of T^* for the N-SmA transition are given in Table II. For 8OCB-aerosil samples, there is a slight increase in T^* up to $\rho_S = 0.051$ g cm^{-3} which is not fully understood. However, above this aerosil density, a sharp drop in T^* is observed on the order of that seen for the 8CB-aerosil system. Also, the recovery and subsequent slower decrease in T^* for $\rho_S \gtrsim 0.1$ appears broader in ρ_S as compared to the 8CB-aerosil samples. Table II also gives the N-I transition temperatures and these track the same trend.

The heat capacity maximum at the pseudotransition is an indication of the finite-size effects that are inherent in such studies. Figure 10 depicts a log-log representation of the heat capacity maximum as a function of ρ_S for the 8OCB and 8CB-aerosil samples, where again the error bars indicate reproducibility. Since the mean distance between silica surfaces scales as ρ_S^{-1}, the construction presented in Fig. 10 should reveal a straight line having a slope equal to $\alpha/\nu_\parallel$ for simple finite-size scaling effects. For pure 8OCB, $\alpha/\nu_\parallel = 0.28$ [8] whereas the slope for the 8OCB-aerosil samples varies from 0.75 for $\rho_S < 0.1$ to 1.77 for $\rho_S > 0.1$. However, as described in detail for the 8CB-aerosil system [4], corrections-to-scaling terms play a significant role and alter the expected finite-size behavior.

A more complete finite-size scaling (FSS) analysis should begin with the power-law form of the excess specific heat given by Eq. (16) and the power-law form describing the correlation length of the ordered phase taken as

$$\xi_\parallel = \xi_{\parallel o} t^{-\nu_\parallel}. \tag{17}$$

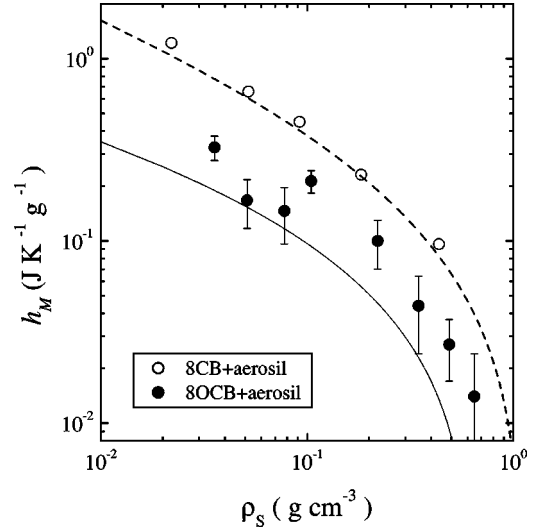For smectic liquid crystals the parallel correlation length is always larger than the perpendicular one, and so our analysis uses this length scale for the definition of the minimum reduced temperature. Defining the maximum possible correlation length as ξ_M, one solves Eq. (17) for the *minimum* reduced temperature above T^* as $t_m^+ = (\xi_M/\xi_{\parallel o})^{-1/\nu_\parallel}$. It is not possible to define a similar minimum reduced temperature below the transition since the correlation length behavior below $T_{N\text{-}A}^0$ is not known. Substituting t_m^+ into Eq. (16) gives the relationship for the heat capacity maximum h_M at the N-SmA transition as a function of the cutoff correlation length as

$$h_M = A^\pm (\xi_M/\xi_{\parallel o})^{\alpha/\nu_\parallel} [1 + D^\pm (\xi_M/\xi_{\parallel o})^{-\Delta_1/\nu_\parallel}] + B_c. \tag{18}$$

Because of the importance of corrections to scaling for the analysis of $\Delta C_p(N\text{-}A)$, a log-log plot of $h_M - B_c$ versus ξ_M would not yield a straight line of slope $\alpha/\nu_\parallel$. The FSS effect on the N-SmA transition enthalpy is obvious since it involves replacing the singular $\Delta C_p(N\text{-}A)$ peak between t_m^+ and t_m^- by h_M and thus decreasing the integral of $\Delta C_p(N\text{-}A)$ over T.

Plotted on Fig. 10 are FSS trends given by Eq. (18) for 8CB-aerosil and 8OCB-aerosil samples using the *bulk* N-SmA 8CB and 8OCB critical parameters, respectively, and the mean distance between silica surfaces (mean void size) $\ell_o = 2/a\rho_S$ [3,4], where a is the specific surface area, for the cutoff correlation length ξ_M. This closely follows the procedure laid out in Ref. [4]. The result for 8CB-aerosil samples are in very good agreement despite the change in the apparent critical behavior of the specific heat. However, this interesting result is not seen in the 8OCB-aerosil samples where the *bulk* finite-size scaling analysis is everywhere lower than that observed. Despite the uncertainty in the 8OCB-aerosil

results, the agreement seen between FSS using the bulk critical parameters and the 8CB-aerosil samples must be regarded as accidental. Also, the change in shape of $\Delta C_p(N\text{-}A)$ described by the changing fit parameters given in Table III is more important than FSS for the enthalpy variation with ρ_S as shown in Fig. 9.

IV. DISCUSSION AND CONCLUSIONS

Results have been presented from high-resolution x-ray scattering and ac-calorimetry experiments on 8OCB-aerosil dispersions. In this section, we compare these results with equivalent experiments on 8CB-aerosil and 8CB-aerogel and with theoretical models.

A. 8OCB-8CB aerosil comparison

A detailed comparison of the behavior of 8OCB and 8CB-aerosil dispersions is illuminating. The x-ray structure factor for liquid-crystal (LC)–aerosil dispersions has been described using a random-field model that accounts well for the data. The correlation length and amplitudes for this model have been presented as a function of the aerosil density ρ_S for each sample. These parameters for 8OCB-aerosil dispersions are fully compatible with existing results for 8CB-aerosil dispersions [1,2]. The dependence of the cube root of the correlation volume at low temperature $\bar{\xi}^{\text{LT}}$ on ρ_S for 8CB and 8OCB is seen in Fig. 7. This shows that the disorder strength experienced by these two liquid crystals is very similar. Perhaps this is no surprise since the two systems have the same polar cyano end groups that are likely to anchor to the aerosil and that the strength of smectic interactions in the two systems is likely to be similar. The higher sensitivity to changes in density for 8OCB [5] appears to have little effect on the results. The small departure of the 8OCB trends from both theory and the 8CB trend at low disorder strength (Fig. 5 and Fig. 7) could possibly be due to the unusual phase diagram for this material. Unlike 8CB, further cooling takes 8OCB back towards the nematic phase. This could lead to a higher sensitivity to disorder in regimes with similar characteristics to the pure material.

The calorimetry results show that the specific heat peak associated with the N-SmA phase transition remains sharp for low disorder while evolving in its critical behavior with increasing ρ_S towards the underlying 3D-XY behavior. See Fig. 8 and Table III. For higher ρ_S samples, the N-SmA transition becomes highly smeared, concomitant with the decreasing correlation volume with increasing ρ_S. The decrease in the transition enthalpy, Fig. 9, and in the specific heat maximum, Fig. 10, with increasing ρ_S is very similar to those observed for the 8CB-aerosil system [4]. However, the shift in the pseudotransition temperature T^* with respect to the pure LC transition temperature between the 8OCB-aerosil and 8CB-aerosil samples, while similar, differs in the quantitative dependence on ρ_S. These results are consistent with the disorder induced by the aerosil gel, altering the coupling between the nematic and smectic phases [4].

The specific heat exponent α reflects the complexity of the pure material transitional behavior [8]. For a wide nematic range α is close to its 3D-XY value whereas a short nematic range leads to tricriticality. The difference in behavior of α between 8OCB-aerosil system, 8CB-aerosil system [3], and 4O.8 [35] is likely to be due to the different initial values. As aerosils are added both systems move towards 3D-XY behavior—the 8CB system starts with a higher α value and hence has to change further to reach the 3D-XY fixed point. The variation of α with ρ_S is thought to be due to changes in the coupling between nematic and smectic phases due to the aerosils [4].

B. Aerosil-aerogel comparison

The x-ray results for 8OCB-aerosil dispersions presented here provide an important comparison with 8CB in an aerogel medium [15,17]. The studies of the aerogel system show the N-SmA transition being destroyed with the line shape corresponding to smectic fluctuations observed to broaden significantly. The temperature dependence of the correlation length and peak amplitude have been compared with expectations for a model of anomalous elasticity [17]. The 8CB-aerogel system is thought to be close to the putative smectic Bragg glass state. Our x-ray scattering measurements are in good agreement with those on 8CB-aerosil dispersions. These aerosil data, contrary to predictions [23], show that the low-temperature correlation length is independent of temperature rather than varying like some power of the pure smectic layer compression modulus $B(T)$. As discussed for 8CB [2], it is surprising that the weaker disorder aerosil system seems to resemble the putative smectic Bragg glass less than the aerogel system [17]. It should be stressed that the analysis used for these LC-aerosil x-ray data differs greatly from that used in Refs. [15,17] to analyze the data for 8CB-aerogel. The approach presented here for 8OCB-aerosil and that for 8CB-aerosil [1,2]. is motivated by the following three key ideas.

(i) The random-field contribution to the structure factor has the form of the thermal contribution squared.

(ii) In a random medium the underlying line shape will be the powder average of the structure factor.

(iii) As the disorder strength decreases, the behavior of the system should converge on pure liquid-crystal behavior.

The first idea is implemented via Eqs. (6), (7), and (11) and, consistent with the second idea, an accurate powder average is evaluated. The third idea is implicit in our thermal and random-field structure factors, Eqs. (6) and (7): the anisotropy and fourth-order correction are assumed to retain the same behavior as for the pure material. In the 8CB-aerogel analysis [15,17] two components to the scattering are also considered, in line with the first idea; however, in all other respects the analysis differs from that presented here and in Refs. [1,2]. For the aerogel analysis in Refs. [15,17], the thermal contribution is taken to be a broad isotropic Lorentzian. The anisotropy, the necessity of powder averaging, and the fourth-order correction are all ignored. For the random-field contribution, the necessity of performing a powder average is considered; however, the scattering is taken to be described by an anisotropic Lorentzian squared, ignoring the

fourth-order correction, and making an approximation to the powder average. The thermal and random-field contributions to the scattering are taken to have different peak positions and correlation lengths. This is inconsistent with theory [23,32,36] and common practice [9,37]. We conclude that a direct comparison of the fit parameters for the aerogel and aerosil results is not possible. The necessity of using the analysis presented here becomes stark and unavoidable as the smectic correlation lengths become increasingly anisotropic (for $\bar{8}$S5 see Fig. 4 in Ref. [2]). It is observed that $\bar{8}$S5-aerosil x-ray scattering is unanalyzable using the protocol employed in Refs. [15,17] (for further details see Ref. [38]).

C. 8*OCB*-aerosil–theory comparison

The observed breakup into finite-sized domains [11,12,39] as well as the characteristics of the line shape [32] are consistent with random-field behavior. Theories of random-field behavior predict the relationship between the saturated correlation length and the random-field variance Δ which depend on the dimensionality of the system and on its lower marginal dimensionality as a random-field system. Since the system is anisotropic, we take the appropriate correlation length for comparison with the theory to be the cube root of the correlation volume at low temperature $\bar{\xi}^{LT}$. For a 3D-XY phase transition, the lower marginal dimensionality, below which long-range order is not possible, is $d_\ell = 2$. Due to the Landau-Peierls instability, the pure N-SmA transition has a lower marginal dimensionality of $d_\ell = 3$. The pioneering observations of the algebraic decay of smectic correlations, a hallmark of a system at its lower marginal dimensionality, were made on pure 8OCB [40]. However, on the length scales accessible in this work, the SmA phase of pure 8OCB is ordered. Indeed, broadening of the peak beyond the resolution limit is unobservable even for $\rho_S = 0.025$ g cm^{-3}. Thus the distinction between a 3D-XY and a N-SmA transition is not important on the length scales probed here; pure smectic ordering can be reasonably thought of as having $d_\ell = 2$. Random-field fluctuations are more effective than thermal fluctuations at destroying an ordered state. They are thought to have the same effect that thermal fluctuations would have in a system with two fewer dimensions. This implies that we should take $d_\ell = 4$ for the N-SmA transition in a random field. The dependence of the correlation length on the random field variance should be $\bar{\xi}^{LT} \sim \Delta^{-1/(d_\ell - d)}$ $= \Delta^{-1}$ [2,4,32]. The results presented in Fig. 7 agree with this relation if $\Delta = \rho_S$. In addition, the density dependence of the ratio of the random field and thermal amplitudes shown in Fig. 5 supports this equality since $a_2/\sigma_1 \sim \Delta^3$ is expected theoretically [4]. The equality between ρ_S and the random-field variance Δ is consistent with a picture in which each additional aerosil particle perturbs the average phase which is favorable for the existing aerosils. For an LC-aerosil system, a smectic region forms away from the aerosil and then grows with decreasing temperature. Eventually the density wave impinges on the gel structure and is perturbed. The proportionality between ρ_S and the surface area of the dispersed aerosil is supported by our analysis of the background scattering.

The suit of characteristics normally associated with random-field behavior leads us to conclude that the dominant form of disorder is that which couples linearly to the order parameter. This suggests that it is the layer position pinning from Eq. (2) which dominates. This would mean that the system is closely analogous to charge-density wave materials where the phase of the density wave is pinned by impurities [12,13].

Radzihovsky and Toner have made a detailed theoretical study of the N-SmA transition in a porous medium [23]. They find that the tilt disorder that the aerosil or aerogel surface creates is the most pernicious form of disorder. This corresponds to the first term in Eq. (2). The results for both 8OCB-aerosil and 8CB-aerosil show that the low-temperature correlation length is independent of temperature. This is contrary to the tilt disorder model which predicts that the correlation length should vary as some power of the pure smectic layer compression modulus $B(T)$. The reasons for the discrepancy between the model [23] and the liquid crystal–aerosil data are not fully understood. Since no current theory successfully captures all of the empirical features of the pure liquid-crystal N-SmA transition, perhaps it is not surprising that there are discrepancies between theory and experiment in the presence of quenched disorder.

The calorimetry measurements presented here and elsewhere [3,35] indicate a systematic trend in the behavior of the smectic fluctuations in a gel. The exponent α is observed to decrease with increasing aerosil density down to a value close to zero. At around this aerosil density the $\Delta C_p(N\text{-}A)$ line shape is substantially rounded and can no longer be described by a power law. The final exponent is consistent with the 3D-XY value of $\alpha_{3\text{D-}XY} = -0.013$. The indication is that the pretransitional fluctuations take on an increasingly 3D-XY character with increasing aerosil concentration. The difference between the pure N-SmA transition and the 3D-XY transition is due to the de Gennes coupling between the nematic and smectic order parameters and the anisotropic coupling between the nematic fluctuations and the smectic order parameter. The calorimetry results strongly suggest that the coupling becomes negligible with increasing aerosil concentration. This trend is corroborated by the deuterium NMR results that show a steady decrease in the ability of the liquid crystal to realign with a rotated magnetic field. There is no capacity to realign and hence no nematic susceptibility when $\rho_S \gtrsim 0.1$ g cm^{-3}. Both calorimetry and DNMR results point towards a steady decrease in the nematic susceptibility as ρ_S increases. This observation suggests that the role for director fluctuations is diminishing approaching the N-SmA transition in the gel. The enhanced role for director fluctuations anticipated under the anomalous elasticity model [23] is inconsistent with this observed trend.

This research opens new directions for study. We have demonstrated that the nematic–smectic-A transition with dispersed aerosil gels represents a random-field system where the disorder strength can be well controlled. Ising symmetry random-field systems have been well studied using the Fishman-Aharony trick. This technique fails, in principle, for continuous symmetry phase transitions. Pinning smectic layer positions with an aerosil gel provides a model system

where the order parameter has a continuous symmetry. This opens a variety of possibilities for studying phase diagrams of continuous symmetry systems. Examples are the reentrant N-SmA-N_r phase diagram of 8OCB:6OCB mixtures and the smectic-A to smectic-C (SmA-SmC) transition for $\bar{8}$S5. In the 8OCB:6OCB mixture, a material with a smectic phase is combined with a material that exhibits only nematic order. Below a critical concentration of 6OCB the smectic phase still exists but melts on cooling into a reentrant nematic (N_r) phase. The role of layer pinning by aerosils on this system is closely analogous to the effect of pinned impurities in the recently observed reentrant vortex system [41]. The SmA-SmC transition in $\bar{8}$S5 is a true 3D-XY transition that has mean-field character due to the Ginzburg criterion. Our studies show how this transition is modified by dispersed aerosils [38].

[1] S. Park, R.L. Leheny, R.J. Birgeneau, J.-L. Gallani, C.W. Garland, and G.S. Iannacchione, Phys. Rev. E **65**, 050703(R) (2002).

[2] R.L. Leheny, S. Park, R.J. Birgeneau, J.-L. Gallani, C.W. Garland, and G.S. Iannacchione, Phys. Rev. E **67**, 011708 (2003).

[3] G.S. Iannacchione, C.W. Garland, J.T. Mang, and T.P. Rieker, Phys. Rev. E **58**, 5966 (1998).

[4] G.S. Iannacchione, S. Park, C.W. Garland, R.J. Birgeneau, and R.L. Leheny, Phys. Rev. E **67**, 011709 (2003).

[5] A.R. Kortan, H. von Kanel, R.J. Birgeneau, and J.D. Litster, J. Phys. (France) **45**, 529 (1984); K.J. Lushington, G.B. Kasting, and C.W. Garland, Phys. Rev. B **22**, 2569 (1980).

[6] P.G. de Gennes and J. Prost, *The Physics of Liquid Crystals*, 2nd ed. (Oxford University Press, New York, 1993).

[7] G.B. Kasting, K.J. Lushington, and C.W. Garland, Phys. Rev. B **22**, 321 (1980).

[8] C.W. Garland and G. Nounesis, Phys. Rev. E **49**, 2964 (1994).

[9] R.J. Birgeneau, J. Magn. Magn. Mater. **177-181**, 1 (1998).

[10] S. Fishman and A. Aharony, J. Phys. C **12**, L729 (1979).

[11] A.I. Larkin and Yu.N. Ovchinnikov, J. Low Temp. Phys. **34**, 409 (1979).

[12] P.A. Lee and T.M. Rice, Phys. Rev. B **19**, 3970 (1979).

[13] J. McCarten, D.A. DiCarlo, M.P. Maher, T.L. Adelman, and R.E. Thorne, Phys. Rev. B **46**, 4456 (1992).

[14] B.M. Ocko, R.J. Birgeneau, J.D. Litster, and M.E. Neubert, Phys. Rev. Lett. **52**, 208 (1984).

[15] A.G. Rappaport, N.A. Clark, B.N. Thomas, and T. Bellini, in *Liquid Crystals in Complex Geometries Formed by Polymer and Porous Networks*, edited by G. P. Crawford and S. Zumer (Taylor and Francis, London, 1996), Chap. 20.

[16] L. Wu, B. Zhou, C.W. Garland, T. Bellini, and D.W. Schaefer, Phys. Rev. E **51**, 2157 (1995).

[17] T. Bellini, L. Radzihovsky, J. Toner, and N.A. Clark, Science **294**, 1074 (2001).

[18] M.J.P. Gingras (private communication).

[19] D.E. Feldman, Phys. Rev. Lett. **84**, 4886 (2000).

[20] T. Bellini, N.A. Clark, V. Degiorgio, F. Mantegazza, and G. Natale, Phys. Rev. E **57**, 2996 (1998).

[21] T. Bellini, M. Buscaglia, C. Chiccoli, F. Mantegazza, P. Pasini, and C. Zannoni, Phys. Rev. Lett. **85**, 1008 (2000).

[22] T. Bellini, M. Buscaglia, C. Chiccoli, F. Mantegazza, P. Pasini, and C. Zannoni, Phys. Rev. Lett. **88**, 245506 (2002).

[23] L. Radzihovsky and J. Toner, Phys. Rev. B **60**, 206 (1999).

[24] T. Jin and D. Finotello, Phys. Rev. Lett. **86**, 818 (2001).

[25] C. Retsch, I. McNulty, and G.S. Iannacchione, Phys. Rev. E **65**, 032701 (2002).

[26] Degussa Corp., Silica Division, 65 Challenger Road, Ridgefield Park, NJ 07660. Technical data are given in Degussa booklet AEROSILS.

[27] A. Guinier, *X-ray Diffraction in Crystals, Imperfect Crystals and Amorphous Bodies* (Freeman, San Francisco, 1963).

[28] H. Yao, K. Ema, and C. W. Garland, Rev. Sci. Instrum. **69**, 172 (1998).

[29] G.S. Iannacchione, S. Qian, D. Finotello, and F.M. Aliev, Phys. Rev. E **56**, 554 (1997).

[30] J.D. Litster, J. Als-Nielsen, R.J. Birgeneau, S.S. Dana, D. Davidov, F. Garcia-Golding, M. Kaplan, C.R. Safinya, and R. Schaetzing, J. Phys. Colloq. **40**, C3 (1979).

[31] G. Parisi and N. Sourlas, Phys. Rev. Lett. **43**, 744 (1979).

[32] A. Aharony and E. Pytte, Phys. Rev. B **27**, 5872 (1983).

[33] Other forms for the background scattering were also tried, but the resulting fit parameters were very similar to those reported here.

[34] R.J. Birgeneau, C.W. Garland, G.B. Kasting, and B.M. Ocko, Phys. Rev. A **24**, 2624 (1981).

[35] H. Haga and C.W. Garland, Liq. Cryst. **22**, 275 (1997).

[36] B. Ward, Ph.D thesis, University of Colorado, 1999 (unpublished).

[37] D.P. Belanger, in *Spin Glasses and Random Fields*, edited by A.P. Young (World Scientific, Singapore, 1997), p. 251.

[38] S. Park, P.S. Clegg, R.L. Leheny, C.W. Garland, G.S. Iannacchione, R.J. Birgeneau, and M.E. Neubert (unpublished).

[39] Y. Imry and S.-K. Ma, Phys. Rev. Lett. **35**, 1399 (1975).

[40] J. Als-Nielsen, J.D. Litster, R.J. Birgeneau, M. Kaplan, C.R. Safinya, A. Lindegaard-Andersen, and S. Mathiesen, Phys. Rev. B **22**, 312 (1980).

[41] N. Avraham, B. Khaykovich, Y. Myasoedov, M. Rappaport, H. Shtrikman, D.E. Feldman, T. Tamegai, P.H. Kes, M. Li, M. Konczykowski, K. van der Beek, and E. Zeldov, Nature (London) **411**, 451 (2001).